Journal of Computational Applied Mechanics 2025, 56(2): 318-330

DOI: 10.22059/jcamech.2025.390563.1371

RESEARCH PAPER

Effects of infill parameter variations on mechanical properties in 3D printed structures: comparative study with fem analysis

Anca Elena Stanciu [a], Andrei Bencze [a], Cristina Cazan [a], Sorin Vlase [a,b] , Marin Marin [c,d, *], Andreas Öchsner [e]

[a] *Transilvania University of Brasov, B-dul Eroilor 29, Brasov, 500036, Romania*
[b] *Institute of Solid Mechanics of Romanian Academy, Str. Constantin Mille no. 15, 030167 Bucharest, Romania*
[c] *Dept of Mathematics and Computer Science, Transilvania University of Brasov, 500036 Brasov, Romania*
[d] *Academy of Romanian Scientists, Ilfov Street 3, Bucharest, 050045, Romania*
[e] *Faculty of Mechanical Engineering, Esslingen University of Applied Sciences, 73728 Esslingen, Germany*

Abstract

This paper investigates the mechanical behavior of 3D-printed Polyethylene Terephthalate Glycol (PETG) and Poly Lactic Acid (PLA). This study aims to provide information on how the mechanical properties of 3D-printed PETG and 3D-printed PLA are affected by the in-fill parameter (printed layer density). Different infill parameters (hereafter named layer density or density) and ply orientation (filament/fiber orientation) are used for obtaining PETG and PLA samples. Values of mechanical properties were recorded at bending tests on specimens with different densities, namely 10%, 15% and 20%, at angles of 0° and 45°, aiming to assess the material's quality about its properties and applications. PETG and PLA exhibited elastoplastic behavior during bending tests. Obtained results indicate that samples made with PLA exhibit superior mechanical properties compared to those made with PETG. The samples bending tests are validated with FEM analysis. PETG-based samples demonstrate higher resilience and elongation at break values, indicating greater flexibility and resistance to deformation. In contrast, PLA-based samples display more brittle characteristics, with elongation values at failure significantly lower by one order of magnitude.

Keywords: bending test; polyethylene terephthalate glycol (PETG); Poly Lactic Acid (PLA); mechanical properties; finite element method FEM;

1. Introduction

3D printing has become extremely popular in the last two decades. Traditional manufacturing methods often involve lengthy and costly processes to create prototypes, whereas 3D printing allows for the efficient and rapid production of prototypes of highly customized and complex geometries that are difficult or even impossible to achieve with traditional manufacturing methods. 3D printing also allows for the creation of intricate internal structures, hollow components, and optimized designs that can enhance the performance of a part. This customization and complexity are particularly valuable in aerospace, healthcare, and architecture industries, where unique designs and tailored solutions are often required.

Modern 3D printing technology offers a wide range of possibilities by using materials in different forms (solid, powder, melt, and liquid) to achieve varying levels of strength and precision [1-3]. Fused deposition modelling (FDM™) stands out among these technologies due to its reliability, cost-effectiveness, and user-friendly nature [4-6].

* Corresponding authors *E-mail address:* m.marin@unitbv.ro

In the traditional configuration of FDM a thermoplastic filament with a consistent diameter is melted and extruded through a nozzle. The size of the nozzle determines the thickness of the printed layers, printing time, and final object resolution [7-11].

The mechanical properties of printed parts are significantly influenced by processing conditions, including extrusion temperature, layer thickness and printing speed [12-14]. Many studies have focused on optimizing process parameters and understanding their impact on the final properties of 3D-printed parts. A significant limitation of 3D printing for practical applications is the availability of suitable materials for specific uses [15, 16].

Extensive research has been conducted on the modelling and characterizing of polymers manufactured using FDM (Fused Deposition Modelling). Various studies have focused on different aspects of FDM-printed polymers. The elastoplastic behavior of FDM-printed polymers has been modelled, considering their structural dependence. These models help understand the printed parts' mechanical response and deformation characteristics [17-22].

Zhao et al. [23] proposed determining the tensile strength and Young's modulus of FDM-printed polymers based on factors like raster angles and layer thicknesses. These models assisted in predicting the mechanical properties of printed parts under tension. Somireddy et al. [24] investigated different length scales and their interactions in FDM-printed polymers, primarily using the classical laminate theory (CLT). However, it is worth noting that CLT assumptions, such as perfect bonding, may have limited validity for FDM.

Tensile experiments have been performed to compare FDM materials, while differences in characterization methods for polymers, particularly tensile testing, have been explored. These studies contribute to understanding the mechanical behavior and performance of different FDM-printed polymers [25]. The influence of processing parameters, such as raster pattern, print orientation, and tensile specimen dimensions, on anisotropy has been investigated using different tensile test specimen geometries based on ASTM D638 standards. The effects of layer thickness and build orientation have been analyzed through tensile, flexural, and impact tests [26, 27]. The mechanical properties of FDM-printed polymers are significantly affected by layer thickness, orientation angles, and air gaps. Researchers have identified this phenomenon and explored its implications [28, 29]. The correlation between 3D printing time and dimensional accuracy has been established through parameter optimization. This research helps optimize printing parameters to achieve desired dimensional accuracy in FDM-printed parts.

FDM™ is particularly advantageous for medium to large sized objects, as it provides a desirable balance between final resolution, printing speed, and material cost. Moreover, FDM™ allows using diverse polymeric and composite materials with different properties.

In the case of the FDM™ process, the most popular, affordable, and user-friendly thermoplastic materials currently available are poly (lactic acid) (PLA) [30-33] and poly (ethylene terephthalate glycol) (PETG) [34-38]. There are also other polymer matrices on the market, such as poly(acrylonitrile-butadiene-styrene) (ABS), 2polyamide (PA), polycarbonate (PC), and thermoplastic polyurethane (TPU). However, these materials have several limitations. For example, PA and PC require high extrusion temperatures, TPU has a low mechanical modulus, ABS and PC can produce toxic chemicals during the melting process, PA and PC have high density, PA and ABS exhibit high levels of shrinkage, and PA and PC may contain unsafe fillers and additives. Some materials, such as PA, PC, and TPU, can be costly [39-42]. PLA and PETG filaments are commonly used for 3D printing. PLA is renowned for its versatility and is widely adopted in various industries due to its biodegradable nature. On the other hand, PETG is known for its durability, strength and ability to withstand significant impacts. PETG is entirely recyclable, like many other thermoplastic materials. It can develop large parts or materials without deforming or altering the product's structure. It is a safe plastic for food applications and is commonly used for containers and beverage bottles.

Despite the variety of filaments available, comprehensive information on their properties is often limited, making it challenging to compare different data sheets. Filament manufacturers often use different test standards or provide incomplete characterizations. Moreover, the data provided often pertains to the raw material, while the mechanical characterization of printed samples is insufficient. Important factors such as molecular weight and distribution variability, viscosity, crystallinity, and additives are not reported. Accurate property measurements are crucial for making material decisions, especially in safety-critical designs like biomedical applications. Further research is needed to develop test standards based on the material's intended use, considering design weaknesses, durability requirements, and safety factors [22, 34, 43-46].

Due to the limited information the producer provides, it is necessary to conduct tests on samples to determine the material's mechanical properties. Like other materials, the mechanical properties of this materials (PLA and PETG) are influenced by various parameters such as printing speed, temperature (both machine and ambient), humidity, infill (layer density), filament diameter, and filament orientation on each layer. See also [47-50].

This study aimed to investigate the infill parameter's impact (named hereafter layer density or density) on mechanical properties. Different layer densities and ply orientations (filament/fiber orientation) were used. The results were compared with those obtained from the FEM analysis.

2. Materials and methods

2.1. Materials

PLA and PETG are two different polymer matrices, and two commercial brands for each polymer were considered: filaments from TreeD Filaments® for PLA, and filaments from Filoalfa® for PETG. The properties of these materials are summarized in Table 1.

Table 1: Properties of PETG and PLA

Properties	PETG	PLA
Melting point [ºC]	245 to 260	150 to 160
Glass transition temperature [ºC]	75-90	60-65
Injection mould temperature [ºC]	200-255	178-248
Density [g/cm^3]	1.27	1.25
Crystallinity	3-11%	<10%
Tensile modulus [GPa]	2.14	3.12
Melt flow [g/min]	0.8	0.6
Modulus of elasticity[GPa]	15.7	3.5

2.2. Samples preparation

For this study, a series of printed test samples are produced, using the Original Prusa i3 MK3S 3D printer. Printing parameters for PETG and PLA filaments were selected, see Table 2. The test sample geometry are:

- Total length L = 84 mm (L is greater than the bending machine outer supports opening),
- Cross-section width w = 10 mm,
- Cross-section thickness t = 4 mm (resulted from overlapping the correspondent number of plies),
- Cross-section area A = 40 mm^2,
- Cross-section moment of inertia (for bending) I = 53.3 mm^4.

Table 2: Printing properties for PETG and PLA filaments

Printing properties	PETG	PLA
Bed temperature [ºC]	90	90
Layer thickness [mm]	0.15	0.15
Infill density	10%,15%,20%	10%,15%,20%
Fan speed	100%	100%
Deposition speed [mm/s]	200	200
Deposition temp [°C]	250	245
Extruder temperature [°C]	230	215
Print speed for perimeters [mm/s]	50	50
Print speed for infill [mm/s]	65	65

Different infill parameters (hereafter named layer density or density) and ply orientation (filament/fiber orientation) are used. Orientation 0 means that the fibers (filament laid by the printing head) are aligned with the test sample's longitudinal direction, Fig.1 and Fig.2. A density of 100% means that all available volume in one ply (each ply has a constant thickness, therefore a volume) is filled with material. A lower density is obtained by increasing the distance between 2 parallel passes of the printer head, leaving some gap between the material fibers.

Samples from PETG and PLA with varying densities, specifically 10 %, 15 % and 20 % at angles of 0° and 45° were 3D printed, to evaluate the material's mechanical properties and structural integrity. Five samples were obtained for each PETG and PLA sample printing density. The obtained values provide insights into the quality of the material in terms of its properties and structure.

Orientation 0º for PLA samples

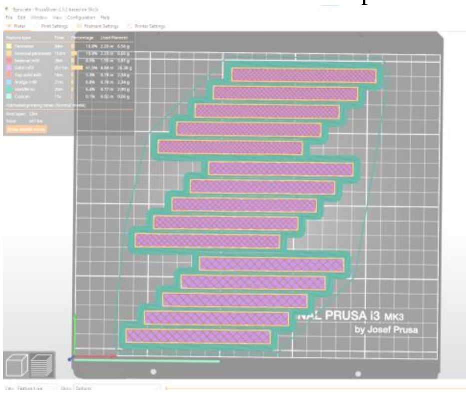

Fig 1: Printing PLA material

Orientation 45º for PETG samples

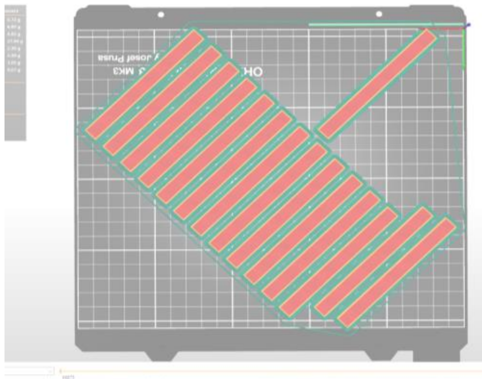

Fig 2: Different filling densities for PETG

2.3. Three-point flexural test

The three-point testing was performed with a Lloyd LR5K Bending Test Machine. The test sample is symmetrically simply supported on two supports distanced at L = 64 mm (L is the effective length), while the load (P) is applied vertically at the center.

The testing machine is produced by Lloyd's Instruments, Great Britain, it is of the LR5K Plus type, Fig. 3, which provides a maximum force Fmax= 5 kN, test speed accuracy: 0.2%; maximum stroke: 840 mm; load resolution: 0.01% of the used force cell; extension resolution: 0.1 micron; force cell: XLC-100K-A1; analysis software: NEXYGEN MT. Two supports and a hemispherical load punch are arranged according to Fig. 3. The alignment of the supports and the spherical punch must be parallel with an accuracy of 0.02 mm.

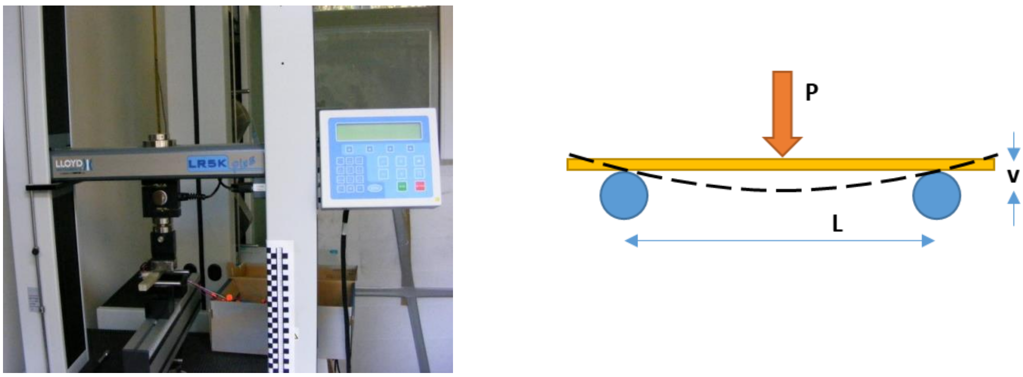

Fig 3: Bending machine inputs and outputs

The machine outputs are applied force P, measured in [N] and the machine extension v, which equals the frame deformation at the center (symmetry line), measured in [mm].

The vertical center loading will subject the test sample to the following:

- Shear load (S), constant on the entire length between the two supports,
- Bending load (Mi), increasing linearly from null at the supports position to a maximum at the center.

The diagram in Fig.4 presents the steps to obtain the desired results. Material strength parameters needed to represent material behavior at the variation of orientation and density are strain, longitudinal elasticity modulus (Young Modulus, E) at the yield limit and yield tensile stress limit (allowable stress).

The method determines the bending behavior of the samples and the tension resistance under bending loading and other aspects related to the stress/strain relationship under the given conditions. The method of placing and testing the specimen is chosen in such a way as to limit shear deformation and avoid interlaminar shear breakage. The sample, supported as a lever, is subjected to bending at a constant rate until it breaks or until the strain reaches a predetermined value. The force applied to the test piece and the arrow (maximum deflection) is measured during the test.

Additionally, the Shear stress can be computed from the inputs:

- Average Shear stress: avr = F/A = cca. 2 MPa at Yield load,
- Peak Shear stress: max = 1.5 F/A = cca. 3 MPa at Yield load, at the center fiber.

The Shear stress can be neglected since its influence, compared to the bending stress at the outer fibers, is small in the total stress.

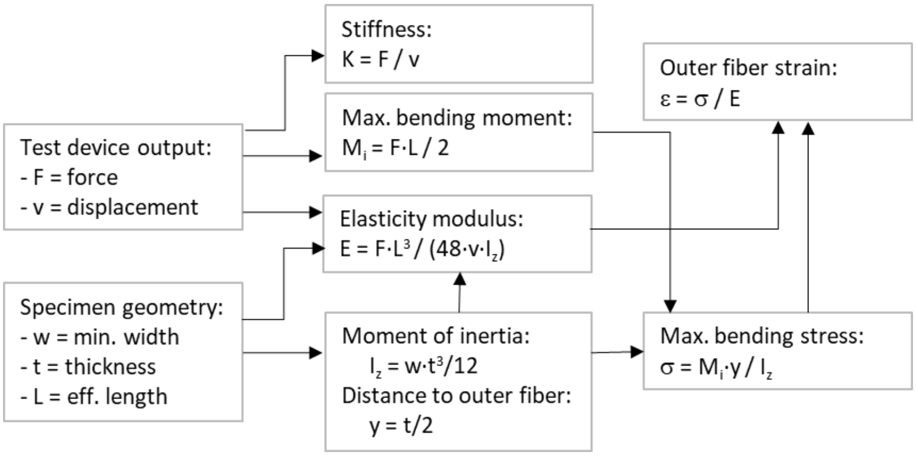

Fig 4: Calculations overview from machine inputs to required outputs

2.4. FE assessment. Model description

The tests on samples are validated with the finite element method.

The finite elements model (FEM) pre-processing and post-processing are realized in MSC Patran 2019, while the static linear analysis (SOL 101) is carried out in MSC Nastran 2019. The mesh is done on the geometry of the surface with 2D Shell elements (with quad4 topology) and has a general global element edge length of 1 mm. The plate thickness defined in the property card is 4 mm. Since the material properties do not vary with the thickness, the shell approach is applicable. For the FE Model, the width is maintained constant on the entire length of the plate.

3. Results and discussions

3.1. Three-point flexural test

Test samples at all orientations and densities present a linear elastic region (important for applications) and then transition into a plastic behavior, where remnant deformations occur. The extension then increases until failure, but the material's loading capabilities decrease abruptly.

Some of the tested samples are shown in Fig.5 and Fig. 6. The typical PETG and PLA material behavior (stress-strain curve) is presented below in Fig. 7.

Fig 5: Orientation 0º for PETG samples, density 15%

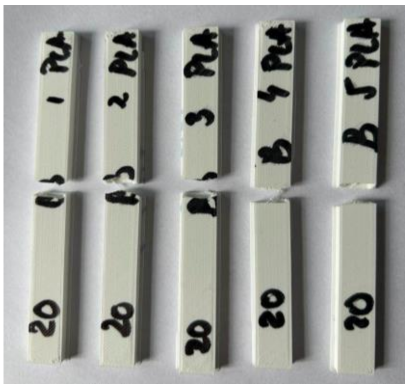

Fig 6: Orientation 45º for PLA samples, density 20%

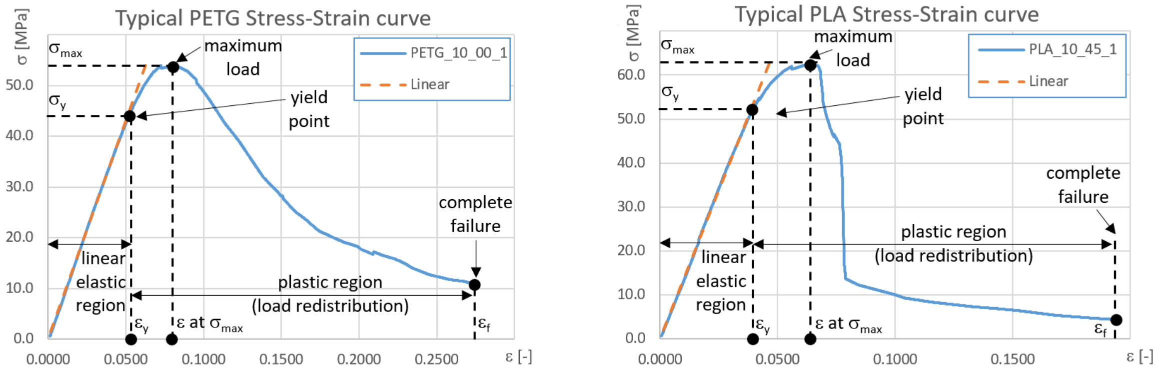

Fig 7: Typical PETG / PLA stress-strain curve

For each sample type for PETG and PLA, the linear elastic region (up to the yield point at σ_y) and the remaining plastic region until maximum loading point (at σ_{max}) can be found on the graph in Fig. 7. In the plastic region, the material is unpredictable due to developing cracks.

The bending test results, for each sample type from PETG and PLA, per each orientation and every tested density, are presented in Fig. 8. The analysis of the average values was followed to ensure the stability of the printed material, without changes occurring in the material, both materials being stable. Both materials exhibited stability. The yield properties of these materials were evaluated both in the longitudinal direction (at 0°) and at a 45° angle. In the longitudinal direction, were obtained maximum values reaching 48.8 MPa at 20% density for PETG and 55.8 MPa at 20% density for PLA. Similarly, at 45° angle, PETG achieved a maximum value of 53.9 MPa at 20% density, while PLA reached 58 MPa at 20% density.

As can be noticed, test samples at all orientations and densities present a linear elastic region, important for applications, and then transition into a plastic behavior, where remnant deformations occur. The extension then increases until failure, but the material's loading capabilities decrease abruptly. Most products' usable industrial region is the linear elastic region. Within this important region, all test samples exhibit a highly uniform behavior. Some test samples present divergence for the maximum and failure loads, stresses, and strains. Still, this behavior can be linked to material quality, uniformity, small and local variations in temperature, density, and other factors.

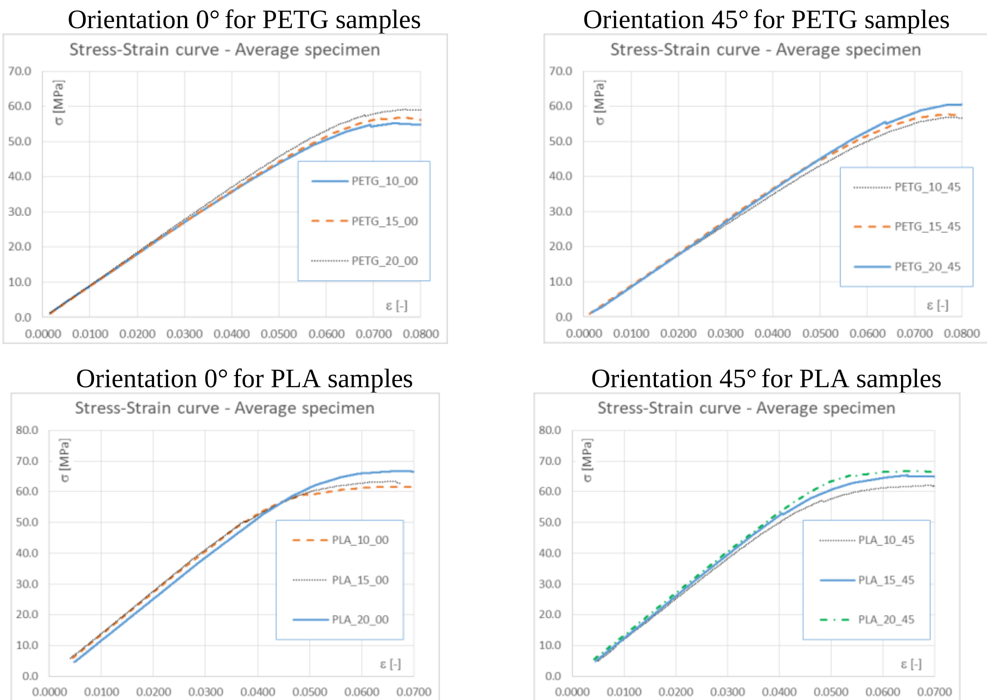

Fig 8: PETG and PLA material properties variation with density

The highest allowable yield tension, represented as Fty (σ_i), is 58 MPa for PLA when measured at a 45° angle, indicating superior bending resistance, as depicted in the Table 3. Notably, this aspect highlights that PETG also reaches its maximum value at 45°, 53.9 MPa. This is attributed to its heightened rigidity, which results in faster material failure at higher densities. Table 4 presents results at material failure (maximum load).

Table 3: Maximum (Max), minimum (Min), average (Avr) values at yield

Material	Orientation	Density	Values at Yield Point								
			σ_i [MPa]			E [MPa]			ε [%]		
			Min	Max	Avr	Min	Max	Avr	Min	Max	Avr
PETG	00	10	41.6	48.0	44.8	848	875	862	0.0483	0.0555	0.0519
		15	40.6	45.9	43.3	835	881	858	0.0479	0.0550	0.0515
		20	46.3	51.4	48.8	876	907	892	0.0523	0.0570	0.0547
	45	10	49.9	53.9	51.9	778	888	833	0.0562	0.0692	0.0627
		15	40.6	48.0	44.3	849	898	874	0.0478	0.0534	0.0506
		20	41.2	48.5	44.8	824	857	840	0.0488	0.0589	0.0538
PLA	00	10	48.5	54.8	51.7	1177	1296	1237	0.0436	0.0481	0.0459
		15	50.3	55.4	52.8	1221	1317	1269	0.0402	0.0458	0.0430
		20	53.8	57.8	55.8	1247	1333	1290	0.0378	0.0440	0.0409
	45	10	49.3	54.4	51.9	1245	1291	1268	0.0413	0.0441	0.0427
		15	50.7	54.6	52.6	1272	1320	1296	0.0387	0.0423	0.0405
		20	54.0	58.0	56.0	1298	1343	1320	0.0380	0.0416	0.0398

Table 4: Maximum (Max), minimum (Min), average (Avr) values at maximum load

Material	Orientation	Density	Values at Maximum Load / Stress								
			σ_i [MPa]			E [MPa]			ε [%]		
			Min	Max	Avr	Min	Max	Avr	Min	Max	Avr
PETG	00	10	53.9	59.1	56.5	669	767	718	0.0727	0.0805	0.0766
		15	52.2	57.3	54.7	621	743	682	0.0765	0.0916	0.0841
		20	57.8	62.2	60.0	736	810	773	0.0753	0.0791	0.0772
	45	10	60.3	61.8	61.1	706	785	746	0.0782	0.0855	0.0818
		15	52.4	60.0	56.2	655	765	710	0.0761	0.0877	0.0819
		20	52.7	58.1	55.4	669	739	704	0.0770	0.0803	0.0786
PLA	00	10	65.8	68.5	67.2	933	1001	967	0.0667	0.0735	0.0701
		15	60.2	64.7	62.5	828	1017	922	0.0592	0.0733	0.0662
		20	63.1	66.8	65.0	906	1035	971	0.0610	0.0734	0.0672
	45	10	62.5	66.2	64.3	928	1008	968	0.0631	0.0685	0.0658
		15	61.1	64.2	62.6	908	986	947	0.0620	0.0704	0.0662
		20	65.9	67.8	66.8	958	1034	996	0.0640	0.0688	0.0664

Considering the properties of the two materials, it can be seen that they have successive values, depending on the density and the longitudinal orientation at 0°. PLA consistently exhibits higher average values for σ_i compared to PETG across all density levels. For instance, at a density of 10%, PLA's values are 15.4% higher, at 15% density, the average σ_i is 21.9% greater, and even at 20% density, PLA maintains a 14.3% advantage over PETG.

At a 45° angle, the average values of the Yield Tension Allowable (σ_i) are also consistently higher for PLA at each density level, even though it matches PETG's value of 51.9 MPa at 10% density. At 15% density, PLA is 18.7% stronger, and at 20% density, it surpasses PETG by 25%. It is advisable to consider these average values for all mechanical properties, as plastic deformation and cracks can manifest within the material.

Comparing the Elastic Modulus (E) for samples created with the 3D printer, we notice that PLA, on average, exhibits roughly 30% more elasticity than PETG. This higher elasticity corresponds to PLA's greater flexibility, even while maintaining proportionality and specific values for each material. In summary, the modulus of elasticity remains largely unaffected by the orientation angle, whether 0° or 45°. The variation in orientation and density primarily influences strain (ε). The average values show minimal variation, ranging between 0.04 and 0.06. This property remains relatively constant for each material, regardless of its density. This underscores the importance of the outer layer in supporting the entire structure.

It's important to note that parameters for mechanical properties can only be determined within a linear environment. When the structure is deformed or the material is damaged in a plastic state, these parameters cannot be accurately identified. Ideally, the material should withstand up to its maximum plastic value.

The longitudinal elasticity modulus E variation with density can be observed in Fig.9, where all values are extracted at a load of F = 40 N (in the linear elastic region before the yielding start). The variation is presented for both 0° and 45° orientations. The machine extension is in direct relation to the strain. Based on these tests, material properties can be extrapolated for higher material densities. Elongation values surpass those of PETG, with an average of 4.6mm. This is primarily due to its significantly lower modulus of elasticity, which hovers around 870MPa. In contrast, PLA exhibits different characteristics, featuring an elongation range between 2.95mm and 3.45mm and a considerably higher modulus of elasticity ranging from 1200MPa to 1400MPa. This results in a 50% increase in elasticity compared to PETG, which remains rigid, while PLA demonstrates a more elastic behavior.

For materials with direction dependent physical properties, for example, elasticity, the specimens must be chosen so that, during the test, the bending stress is applied in the same direction as that in which the products are required in service. If, in an application, the material is subjected to stress in a specific direction relative to the principal direction, it is recommended that the material be tested in this direction.

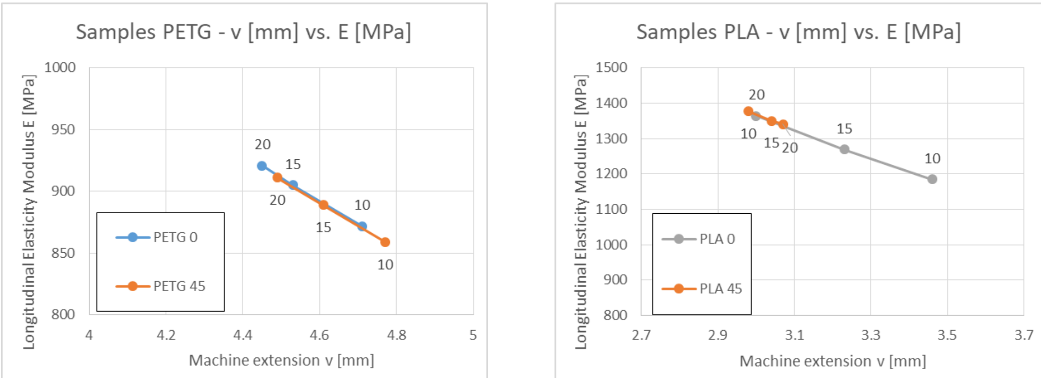

Fig 9: PETG and PLA elasticity modulus E vs. machine extension v - variation with density

The PETG material properties variation with the material density, 0° and 45°, are presented in Fig 10.

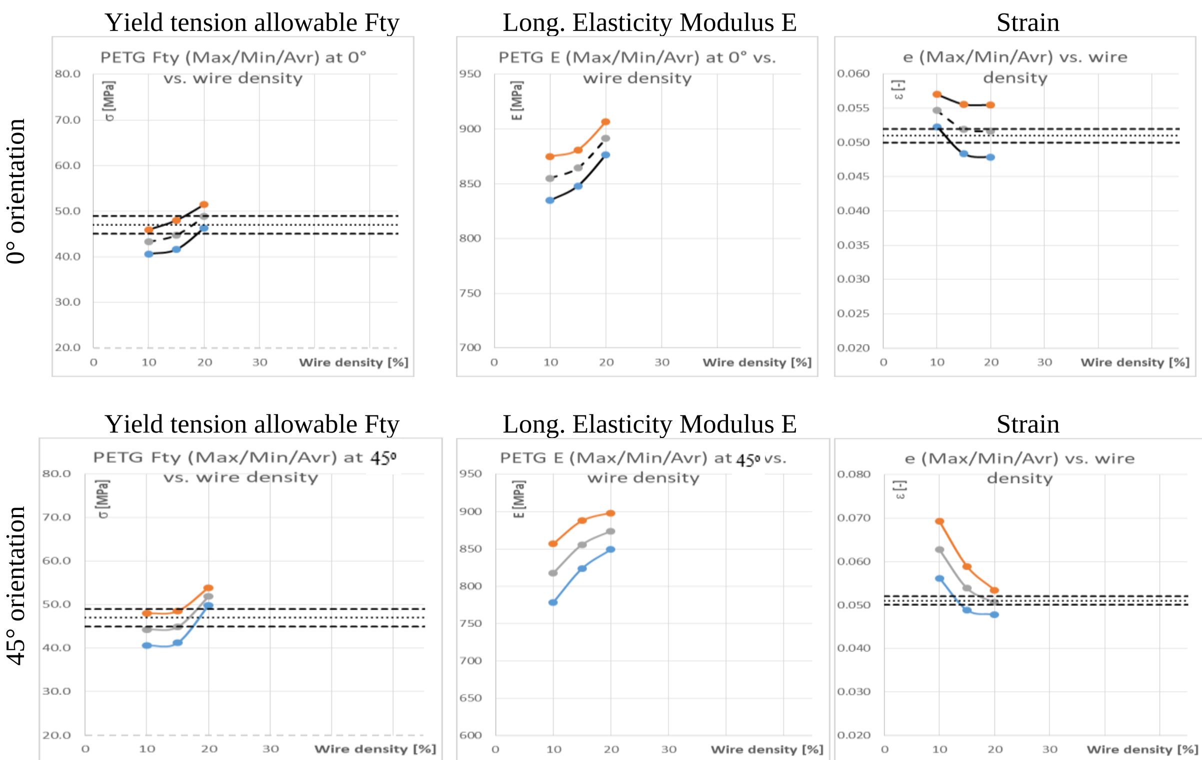

Fig 10: PETG Material properties variation with density, for 0° and 45° orientation

For PETG, the minimum, maximum and average values obtained in the sample tests are presented for all graphs. The horizontal line is only for reference and represents the maximum, minimum and average values provided by the material manufacturer. In the case of PETG at 0°, the yield tension allowable Fty falls within the range of 40 to 51 MPa, while PETG at 45° achieves an approximate value of 54 MPa, slightly higher. The Longitudinal Elasticity Modulus E starts at 830 MPa for 0° and reaches up to 900 MPa for both angles. The Strain for PETG at 0° has a maximum of 0.056, whereas at 45°, it extends even further, reaching up to 0.070.

The PLA material properties variation with the material density, 0° and 45°, are presented in Fig 11. The minimum, maximum and average values obtained in the sample tests are presented for all graphs. The yield tension allowable Fty increases for PLA, ranging between 49 and 59 MPa, regardless of the angle. This indicates that the material maintains a consistent level of strength, regardless of how the fibers are oriented. Regarding Longitudinal Elasticity Modulus E, PLA exhibits significantly higher values, starting at 1170 MPa for 0° and reaching up to 1340 MPa for both angles. This demonstrates its remarkable stiffness and resilience. Regarding Strain, for PLA at 0°, it reaches a maximum of 0.049, while at 45°, it only reaches 0.044, at which point the material experiences a sudden breakage.

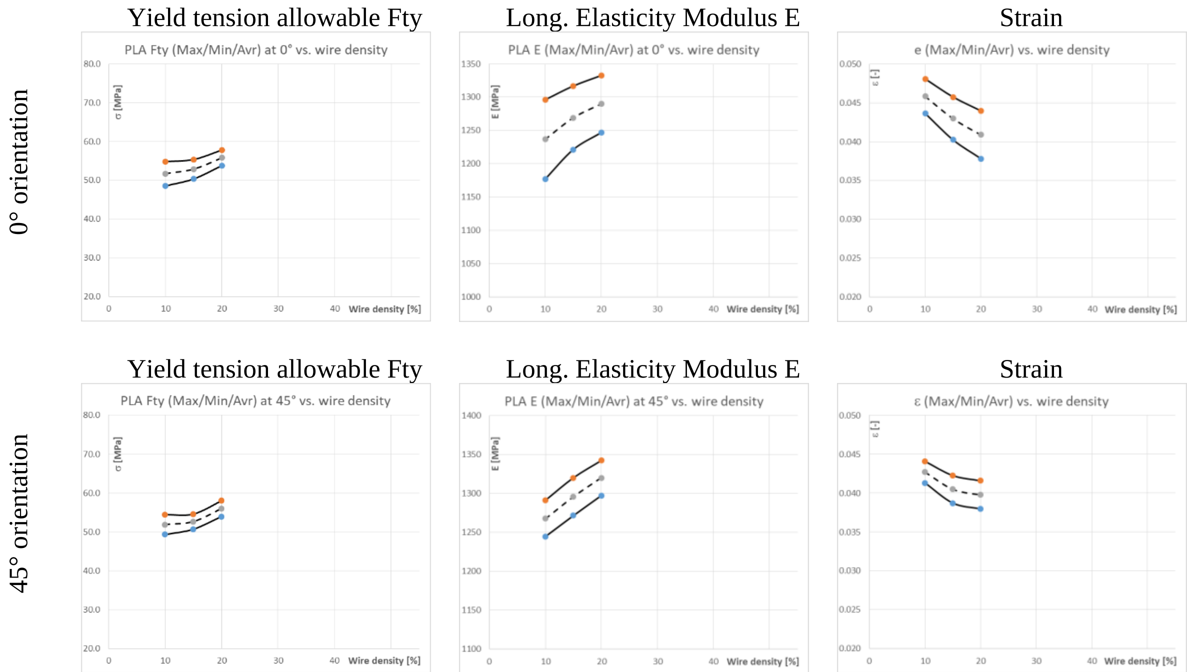

Fig 11: PLA Material properties variation with density, for 0° and 45° orientation

3.2. FE Assessment

The selected material is an isotropic material based on the material properties (Young Modulus) obtained in the previous sample testing stage. The longitudinal Elasticity Modulus is extracted from the linear elastic region for the material with 20% density (see Fig. 12: PETG Elasticity Modulus E vs. Machine Extension v - variation with density):

for 0 degrees orientation: E = 920 MPa.
for 45 degrees orientation: E = 910 MPa.

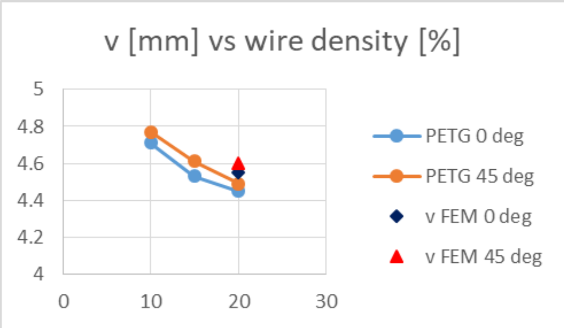

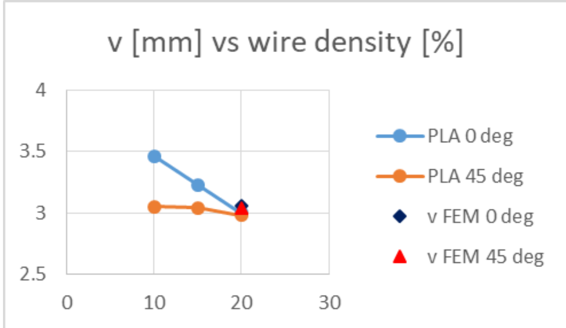

Fig 12: Comparison FE model (20% density) vs. test results for PETG and PLA materials

The load and boundary conditions are done in such a way as to reflect the geometry of the bending machine used in the previous sample testing stage. The applied load (P = 40 N, divided equally between the 11 nodes on the middle symmetry line, see area A) are presented in Fig. 13. For the nodes at the location of the supports, the Degree Of Freedom (DOF) 3 (vertical Z translation) and DOFs 4 and 6 (rotation about X and Z axis) are blocked (see areas B1 and B2). Additionally, the center line of the model (see area A) has DOF 1 (translation on X axis) blocked (see Area A). This is needed to keep the model in place but has no effect on the results.

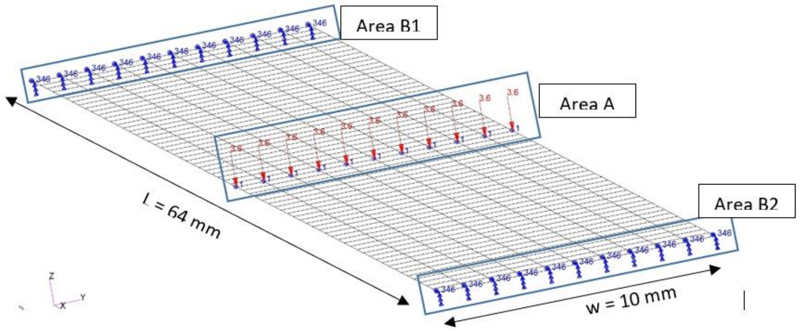

Fig 13: FE plate geometry, mesh and boundary conditions

At post-processing, the combined von Mises stresses and the displacement at the symmetry line are extracted for each orientation and the results are shown in Fig. 14 and then compared with the test results in Fig. 12.

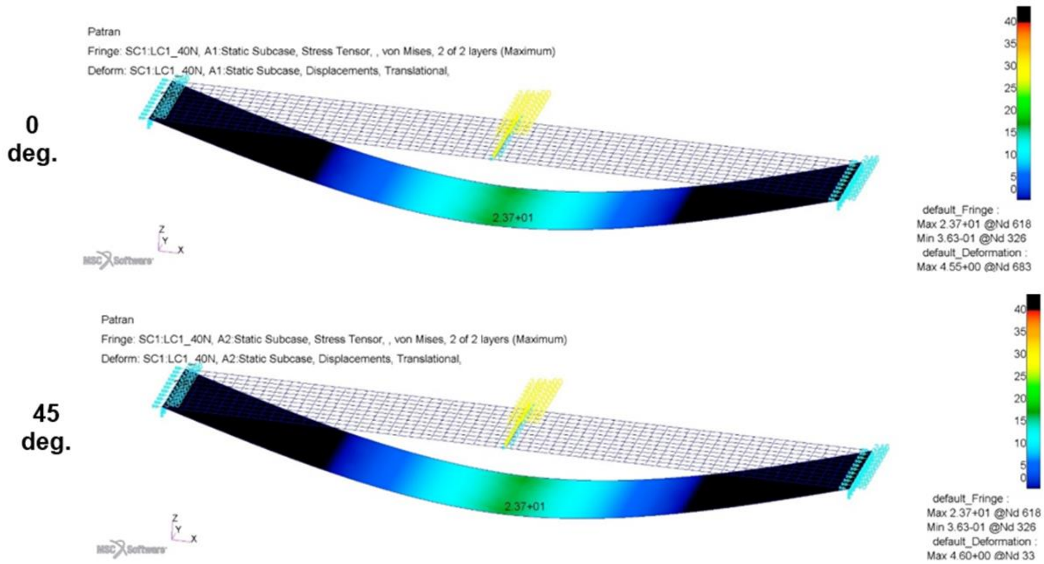

Fig 14: FE model (20% density) results

The differences between test results and FEM results are below 2%, which is acceptable.

4. Conclusions

This study delved into the mechanical behavior of 3D-printed PETG and PLA, focusing on the influence of infill parameters and ply orientation.

The results of the bending tests demonstrate the stability of PETG and PLA materials across different densities and orientations. This stability is fundamental in 3D printing, ensuring the printed material retains its structural integrity without significant changes. When evaluated both in the longitudinal direction (0°) and at a 45° angle, the properties of these materials reveal an increase in strength, with distinct maximum values for each structure. The comparison of PETG and PLA materials reveals intriguing variations in their mechanical properties. While the density ratio remains consistent in the longitudinal direction, PETG and PLA exhibit different maximum yield tension values. These discrepancies underscore the significant impact of material composition, orientation, and density on the mechanical properties of these materials. This observation emphasizes the importance of considering these factors when choosing a material for a specific application or design, as they can substantially influence the material's performance.

The substantial differences in yield tension and modulus of elasticity between PETG and PLA are noteworthy. PLA excels in bending resistance with a yield tension of 58 MPa at a 45° angle, while PETG, despite its high rigidity, demonstrates quicker material failure at higher densities. The study underscores the clear impact of density on material properties, with PETG being less elastic than PLA, making PLA about 30% more elastic than PETG. These distinctions are crucial for evaluating the suitability of these materials for specific applications.

Additionally, finite element analysis (FEA) is an efficient approach for understanding the behavior of these materials in different orientations and densities. By inputting material data into the FEA software, it is possible to model and analyze the behavior of the structures, reducing the need for extensive experimental testing.

This study highlight the significance of material composition, density, and orientation on material behavior. The knowledge gained from this study can inform material selection for specific applications and guide the development of more reliable and predictable 3D-printed structures. Understanding the transition from the linear elastic region to the plastic region is essential for ensuring the integrity and performance of 3D-printed products.

References

[1] A. Chadha, M. I. Ul Haq, A. Raina, R. R. Singh, N. B. Penumarti, M. S. Bishnoi, Effect of fused deposition modelling process parameters on mechanical properties of 3D printed parts, *World Journal of Engineering,* Vol. 16, No. 4, pp. 550-559, 2019.

[2] A. Kichloo, A. Raina, M. I. Ul Haq, M. Wani, Impact of Carbon Fiber Reinforcement on Mechanical and Tribological Behavior of 3D-Printed Polyethylene Terephthalate Glycol Polymer Composites—An Experimental Investigation, *Journal of Materials Engineering and Performance,* Vol. 31, 09/24, 2021.

[3] O. Abdulhameed, A. Al-Ahmari, W. Ameen, S. H. Mian, Additive manufacturing Challenges, trends, and applications, *Advances in Mechanical Engineering,* Vol. 11, pp. 1–27, 02/24, 2019.

[4] S. C. Daminabo, S. Goel, S. A. Grammatikos, H. Y. Nezhad, V. K. Thakur, Fused deposition modeling-based additive manufacturing (3D printing): techniques for polymer material systems, *Materials Today Chemistry,* Vol. 16, pp. 100248, 2020/06/01/, 2020.

[5] K. Krieger, N. Bertollo, M. Dangol, J. Sheridan, M. Lowery, E. o'cearbhaill, Simple and customizable method for fabrication of high-aspect ratio microneedle molds using low-cost 3D printing, *Microsystems & Nanoengineering,* Vol. 5, 12/01, 2019.

[6] I. Solomon, S. Pandian, G. Jagadeesan, A review on the various processing parameters in FDM, *Materials Today: Proceedings,* Vol. 37, 06/01, 2020.

[7] A. Dey, N. Yodo, A Systematic Survey of FDM Process Parameter Optimization and Their Influence on Part Characteristics, *Journal of Manufacturing and Materials Processing,* Vol. 3, pp. 64, 07/29, 2019.

[8] N. A. S. Mohd Pu'ad, R. H. Abdul Haq, H. Mohd Noh, H. Z. Abdullah, M. I. Idris, T. C. Lee, Review on the fabrication of fused deposition modelling (FDM) composite filament for biomedical applications, *Materials Today: Proceedings,* Vol. 29, pp. 228-232, 2020/01/01/, 2020.

[9] S. Bhagia, K. Bornani, R. Agrawal, A. Satlewal, J. Ďurkovič, R. Lagaňa, M. Bhagia, C. G. Yoo, X. Zhao, V. Kunc, Y. Pu, S. Ozcan, A. J. Ragauskas, Critical review of FDM 3D printing of PLA biocomposites filled with biomass resources, characterization, biodegradability, upcycling and opportunities for biorefineries, *Applied Materials Today,* Vol. 24, pp. 101078, 2021/09/01/, 2021.

[10] A. Dey, I. N. Roan Eagle, N. Yodo, A Review on Filament Materials for Fused Filament Fabrication, *Journal of Manufacturing and Materials Processing,* Vol. 5, No. 3, pp. 69, 2021.

[11] A. Woern, D. Byard, R. Oakley, M. Fiedler, S. Snabes, J. Pearce, Fused Particle Fabrication 3-D Printing: Recycled Materials' Optimization and Mechanical Properties, *Materials,* Vol. 11, pp. 1413, 08/12, 2018.

[12] S. Rouf, A. Raina, M. I. Ul Haq, N. Naveed, S. Jeganmohan, A. Kichloo, 3D Printed Parts and Mechanical Properties: Influencing Parameters, Sustainability Aspects, Global Market Scenario, Challenges and Applications, *Advanced Industrial and Engineering Polymer Research,* Vol. 5, 02/01, 2022.

[13] J. Sedlak, Z. Joska, L. Hrbáčková, E. Jurickova, D. Hrušecká, O. Horak, Determination of Mechanical Properties of Plastic Components Made by 3D Printing, *Manufacturing Technology,* Vol. 22, 12/09, 2022.

[14] Z. Joska, L. Andrés, T. Dražan, K. Manas, Z. Pokorný, J. Sedlak, Influence of the shape of the filling on the mechanical properties of samples made by 3D printing, *Manufacturing Technology,* Vol. 21, 03/22, 2021.

[15] J. R. Dizon, A. Espera, Q. Chen, R. Advincula, Mechanical Characterization of 3D-Printed Polymers, *Additive Manufacturing,* Vol. 20, 12/01, 2017.

[16] S. F. Iftekar, A. Aabid, A. Amir, M. Baig, Advancements and Limitations in 3D Printing Materials and Technologies: A Critical Review, *Polymers,* Vol. 15, pp. 2519, 05/30, 2023.

[17] A. Garg, A. Bhattacharya, An Insight to the Failure of FDM Parts under Tensile Loading: Finite Element Analysis and Experimental Study, *International Journal of Mechanical Sciences,* Vol. 120, 12/01, 2016.

[18] A. Raina, M. I. U. Haq, M. Javaid, S. Rab, A. Haleem, 4D Printing for Automotive Industry Applications, *Journal of The Institution of Engineers (India): Series D,* Vol. 102, No. 2, pp. 521-529, 2021/12/01, 2021.

[19] N. Naveed, Investigate the effects of process parameters on material properties and microstructural changes of 3D-printed specimens using fused deposition modelling (FDM), *Materials Technology,* Vol. 36, pp. 1-14, 05/05, 2020.

[20] M. I. U. Haq, A. Raina, M. J. Ghazali, M. Javaid, A. Haleem, *Potential of 3D Printing Technologies in Developing Applications of Polymeric Nanocomposites*, in: H. Jena, J. K. Katiyar, A. Patnaik, *Tribology of Polymer and Polymer Composites for Industry 4.0*, Eds., pp. 193-210, Singapore: Springer Singapore, 2021.

[21] K. Monkova, P. Monka, J. Vanca, M. Zaludek, O. Suba, 2020, *Tensile Behaviour of a 3D Printed Lattice Structure*,

[22] Y. Liao, C. Liu, B. Coppola, G. Barra, L. Di Maio, L. Incarnato, K. Lafdi, Effect of Porosity and Crystallinity on 3D Printed PLA Properties, *Polymers,* Vol. 11, pp. 1487, 09/12, 2019.

[23] Y. Zhao, Y. Chen, Y. Zhou, Novel mechanical models of tensile strength and elastic property of FDM AM PLA materials: Experimental and theoretical analyses, *Materials & Design,* Vol. 181, pp. 108089, 2019/11/05/, 2019.

[24] M. Somireddy, A. Czekanski, Mechanical Characterization of Additively Manufactured Parts by FE Modeling of Mesostructure, *Journal of Manufacturing and Materials Processing,* Vol. 1, pp. 18, 11/13, 2017.

[25] L. Warnung, S.-J. Estermann, A. Reisinger, Mechanical Properties of Fused Deposition Modeling (FDM) 3D Printing Materials, *RTe Journal*, 12/01, 2018.

[26] M. Amirruddin, K. Ismail, T. C. Yap, Effect of layer thickness and raster angle on the tribological behavior of 3D printed materials, *Materials Today: Proceedings,* Vol. 48, pp. 1821-1825, 01/01, 2022.

[27] A. Torrado, D. Roberson, Failure Analysis and Anisotropy Evaluation of 3D-Printed Tensile Test Specimens of Different Geometries and Print Raster Patterns, *Journal of Failure Analysis and Prevention,* Vol. 16, 01/14, 2016.

[28] B. H. Lee, J. Abdullah, Z. Khan, Optimization of Rapid Prototyping Parameters for Production of Flexible ABS Object, *Journal of Materials Processing Technology,* Vol. 169, pp. 54-61, 10/01, 2005.

[29] A. K. Sood, R. K. Ohdar, S. S. Mahapatra, Parametric Appraisal of Mechanical Property of Fused Deposition Modelling Processed Parts, *Materials and Design,* Vol. 31, pp. 287-295, 01/31, 2010.

[30] M. Moradi, A. Aminzadeh, D. Rahmatabadi, A. Hakimi, Experimental investigation on mechanical characterization of 3D printed PLA produced by fused deposition modeling (FDM), *Materials Research Express*, Vol. 8, 03/01, 2021.

[31] J. M. Chacón, M. A. Caminero, E. García-Plaza, P. J. Núñez, Additive manufacturing of PLA structures using fused deposition modelling: Effect of process parameters on mechanical properties and their optimal selection, *Materials & Design*, Vol. 124, pp. 143-157, 2017/06/15/, 2017.

[32] A. Al-Tamimi, A. Pandžić, E. Kadric, Investigation and Prediction of Tensile, Flexural, and Compressive Properties of Tough PLA Material Using Definitive Screening Design, *Polymers,* Vol. 15, pp. 4169, 10/20, 2023.

[33] S. Cicero, M. Sánchez, S. Arrieta, Predicting Critical Loads in Fused Deposition Modeling Graphene-Reinforced PLA Plates Containing Notches Using the Point Method, *Polymers,* Vol. 15, No. 18, pp. 3797, 2023.

[34] M. Kováčová, J. Kozakovičová, M. Prochazka, I. Janigová, M. Vysopal, I. Černičková, J. Krajčovič, Z. Spitalsky, Novel Hybrid PETG Composites for 3D Printing, *Applied Sciences,* Vol. 10, pp. 3062, 04/28, 2020.

[35] E. Soleyman, M. Aberoumand, D. Rahmatabadi, K. Soltan Mohammadi, I. Ghasemi, M. Baniassadi, K. Abrinia, M. Baghani, Assessment of controllable shape transformation, potential applications, and tensile shape memory properties of 3D printed PETG, *Journal of Materials Research and Technology,* Vol. 18, 04/01, 2022.

[36] Ș.-D. Sava, N. Lohan, B. Pricop, P. Mihai, N. Cimpoesu, R.-I. Comăneci, L.-G. Bujoreanu, On the Thermomechanical Behavior of 3D-Printed Specimens of Shape Memory R-PETG, *Polymers,* Vol. 15, pp. 2378, 05/19, 2023.

[37] L. Lopes, D. Reis, A. Paula Junior, M. Almeida, Influence of 3D Microstructure Pattern and Infill Density on the Mechanical and Thermal Properties of PET-G Filaments, *Polymers,* Vol. 15, No. 10, pp. 2268, 2023.

[38] A. Jreije, S. K. Mutyala, B. G. Urbonavičius, A. Šablinskaitė, N. Keršienė, J. Puišo, Ž. Rutkūnienė, D. Adlienė, Modification of 3D Printable Polymer Filaments for Radiation Shielding Applications, *Polymers,* Vol. 15, No. 7, pp. 1700, 2023.

[39] A. Portoaca, R. G. Ripeanu, A. Dinita, M. Tanase, Optimization of 3D Printing Parameters for Enhanced Surface Quality and Wear Resistance, *Polymers,* Vol. 15, pp. 3419, 08/16, 2023.

[40] M. Petousis, I. Ntintakis, K. David, D. Sagris, N. Nasikas, A. Korlos, A. Moutsopoulou, N. Vidakis, A Coherent Assessment of the Compressive Strain Rate Response of PC, PETG, PMMA, and TPU Thermoplastics in MEX Additive Manufacturing, *Polymers,* Vol. 15, 09/28, 2023.

[41] D. Kalas, K. Sima, P. Kadlec, R. Polansky, R. Soukup, J. Reboun, A. Hamacek, FFF 3D Printing in Electronic Applications: Dielectric and Thermal Properties of Selected Polymers, *Polymers,* Vol. 13, pp. 3702, 10/27, 2021.

[42] N. Vidakis, M. Petousis, A. Korlos, E. Velidakis, N. Mountakis, C. Charou, A. Myftari, Strain Rate Sensitivity of Polycarbonate and Thermoplastic Polyurethane for Various 3D Printing Temperatures and Layer Heights, *Polymers,* Vol. 13, 08/17, 2021.

[43] D. S, N. Shetty, Investigation of mechanical properties and applications of polylactic acids – a review, *Materials Research Express,* Vol. 6, 09/19, 2019.

[44] A. Yonezawa, A. Yamada, Deterioration of the Mechanical Properties of FFF 3D-Printed PLA Structures, *Inventions,* Vol. 6, pp. 1, 12/22, 2020.

[45] P. Latko-Durałek, K. Dydek, A. Boczkowska, Thermal, Rheological and Mechanical Properties of PETG/rPETG Blends, *Journal of Polymers and the Environment,* Vol. 27, 11/01, 2019.

[46] A. Özen, D. Auhl, C. Völlmecke, J. Kiendl, B. Abali, Optimization of Manufacturing Parameters and Tensile Specimen Geometry for Fused Deposition Modeling (FDM) 3D-Printed PETG, *Materials,* Vol. 14, pp. 2556, 05/14, 2021.

[47] M. Marin, C. Marinescu, Thermoelasticity of initially stressed bodies, asymptotic equipartition of energies, *International Journal of Engineering Science,* Vol. 36, No. 1, pp. 73-86, 1998/01/01/, 1998.

[48] M. Marin, I. Abbas, R. Kumar, Relaxed Saint-Venant principle for thermoelastic micropolar diffusion, *Structural Engineering and Mechanics,* Vol. 51, pp. 651-662, 08/25, 2014.

[49] M. M. Bhatti, M. Marin, R. Ellahi, I. M. Fudulu, Insight into the dynamics of EMHD hybrid nanofluid (ZnO/CuO-SA) flow through a pipe for geothermal energy applications, *Journal of Thermal Analysis and Calorimetry,* Vol. 148, No. 24, pp. 14261-14273, 2023/12/01, 2023.

[50] A. Yadav, E. Carrera, M. Marin, M. Othman, Reflection of hygrothermal waves in a Nonlocal Theory of coupled thermo-elasticity, *Mechanics of Advanced Materials and Structures,* Vol. 31, pp. 1-14, 10/12, 2022.